Supplementary Information: Electronic and magnetic properties of the RuX_3 (X=Cl, Br, I) family: Two siblings — and a cousin?

David A. S. Kaib,[1,*] Kira Riedl,[1,†] Aleksandar Razpopov,[1] Ying Li,[2] Steffen Backes,[3] Igor I. Mazin,[4] and Roser Valentí[1,‡]

[1] *Institut für Theoretische Physik, Goethe-Universität, 60438 Frankfurt am Main, Germany*
[2] *Department of Applied Physics and MOE Key Laboratory for Nonequilibrium Synthesis and Modulation of Condensed Matter, School of Physics, Xi'an Jiaotong University, Xi'an 710049, China*
[3] *CPHT, CNRS, Ecole Polytechnique, Institut Polytechnique de Paris, Route de Saclay, 91128 Palaiseau, France*
[4] *Department of Physics and Astronomy, George Mason University, Fairfax, Virginia 22030, United States*

(Dated: July 4, 2022)

Supplementary Note 1: Overview of experimental specific heat data

In Supplementary Fig. 1 we show a comparative overview of the low-temperature specific heat data for the RuX_3 family, with data extracted from plots of Supplementary Refs. 1–4. The specific heat for $RuCl_3$ displays a well-defined peak at $T_N \approx 7\,K$ denoting the onset of the zigzag order, while the onset of long-range magnetic order in $RuBr_3$ is observed by a kink at $T_N = 34\,K$ [2] (not within plot range of Supplementary Fig. 1). None of this is observed for the RuI_3 measurements [3, 4].

Supplementary Note 2: Crystal structural details

The structural details for $RuCl_3$ (C2/m [5] and $R\bar{3}$ [6]), $RuBr_3$ ($R\bar{3}$ [2]), and RuI_3 ($R\bar{3}$ [3]) are summarized in Supplementary Table 1. For $RuCl_3$, some reports are indicating the low-temperature structures of C2/m symmetry [5, 7], while others report $R\bar{3}$ structure symmetry [6, 8]. Given the fragility and easy deformability of the van-der-Waals layering, it is plausible that the structures may vary qualitatively between different samples of $RuCl_3$, and the same can be expected for the new members of the RuX_3 family. Recent measurements on $RuBr_3$ [2] indicate a $R\bar{3}$ symmetry, while for RuI_3, crystals with $R\bar{3}$ [3] and $P\bar{3}1c$ [4] symmetries have been grown. For our electronic structure calculations we consider the experimentally reported C2/m and $R\bar{3}$ structures for $RuCl_3$, and the suggested $R\bar{3}$ structures for $RuBr_3$ and RuI_3. Since the $R\bar{3}$ structure of $RuCl_3$ yielded very similar results and the same conclusions as the C2/m structure, we only presented the C2/m results in the main text. The magnetic model extracted for the $R\bar{3}$ structure is given in Supplementary Table 3.

	$RuCl_3$	$RuBr_3$	RuI_3
	C2/m	$R\bar{3}$	$R\bar{3}$	$R\bar{3}$
a (Å)	5.981	5.973	6.296	6.791
b (Å)	10.354	5.973	6.296	6.791
c (Å)	6.014	16.93	17.911	19.026
Ru-Ru (Å)	3.448 (3.454)	3.449	3.635	3.921
Ru-X-Ru	93.6° (93.9°)	94.10°	92.71°	94.13°
Ru-X (Å)	2.36	2.36	2.51	2.68
	2.35	2.35	2.52	2.67

Supplementary Table 1. **Crystallographic structural details.** The structures are obtained from references 2, 3, 5, and 6. In the C2/m structure the values are for Z_1 bonds (X_1/Y_1 bonds).

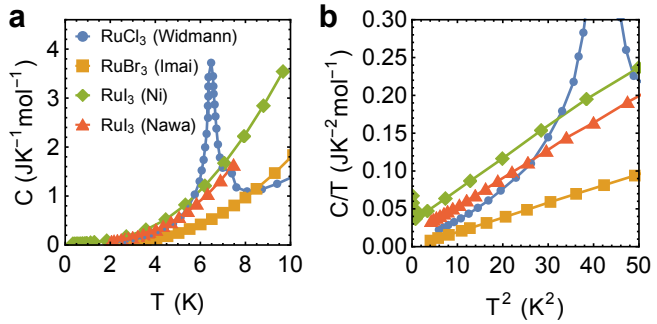

Supplementary Figure 1. **Specific heat C for various reported samples. a** C versus T, **b** C/T versus T^2. Data was extracted from plots in the following references and labelled by respective first-author names: $RuCl_3$ (Widmann) [1], $RuBr_3$ (Imai) [2], RuI_3 (Ni) [3], RuI_3 (Nawa) [4].

Supplementary Note 3: Magnetic ground state properties within DFT

In Supplementary Table 2 we compare measured magnetic properties (subscript "exp") [2–4, 9] to results from total-energy GGA+SOC+U calculations ("DFT") and with exact diagonalization ("ED") results of the pseudospin models of Fig. 5 in the main manuscript. ϕ_M and θ_M characterize the ordered moment direction, as defined in Fig. 1b of the main manuscript. In the case of RuI_3, different magnetic orders and moment directions are extremely close in energy, with Néel AFM or Zigzag order as lowest states, while in ED the

* kaib@itp.uni-frankfurt.de
† riedl@itp.uni-frankfurt.de
‡ valenti@itp.uni-frankfurt.de

	$RuCl_3$	$RuBr_3$	RuI_3
GS_{exp}	Zigzag	Zigzag	metal?
$\theta_{M,exp}$	32°	64°	–
$\phi_{M,exp}$	90°	90°	–
GS_{DFT}	Ferro	Zigzag	Néel/Zigzag
$\theta_{M,DFT}$	0°	5°	
$\phi_{M,DFT}$	0°	86°	
$M_{DFT}(\mu_B)$	0.67	0.47	0.22
$\delta E_{DFT}^{FM\text{-}GS}$(meV/Ru)	0	73.61	26.15
$\delta E_{DFT}^{ZZ\text{-}GS}$(meV/Ru)	3.26	0	0.95
$\delta E_{DFT}^{NL\text{-}GS}$(meV/Ru)	12.08	6.27	0
$\delta E_{DFT}^{ST\text{-}GS}$(meV/Ru)	11.08	118.14	22.41
GS_{ED}	Zigzag	Zigzag	QSL?
$\theta_{M,ED}$	34.4°	32.4°	
$\phi_{M,ED}$	90°	90°	

Supplementary Table 2. **Magnetic ground state (GS) properties of the RuX_3 family.** Experiment (subscript "exp") [2–4, 9] vs total-energy GGA+SOC+U via VASP (with $U_{eff} = 1.5$ eV) results (subscript "DFT") vs solving magnetic models of Fig. 5 in the main manuscript with exact diagonalization ("ED"). The angles θ_M and ϕ_M describe the direction of the magnetic ordered moment, see Fig. 1b,c in the main manuscript. We define $\delta E_{DFT}^{i\text{-}GS}$ as the energy difference between the state i [i = FM (ferromagnetic), ZZ (Zigzag AFM), NL (Néel AFM), ST (stripy AFM)] and the ground state estimated within DFT total energies.

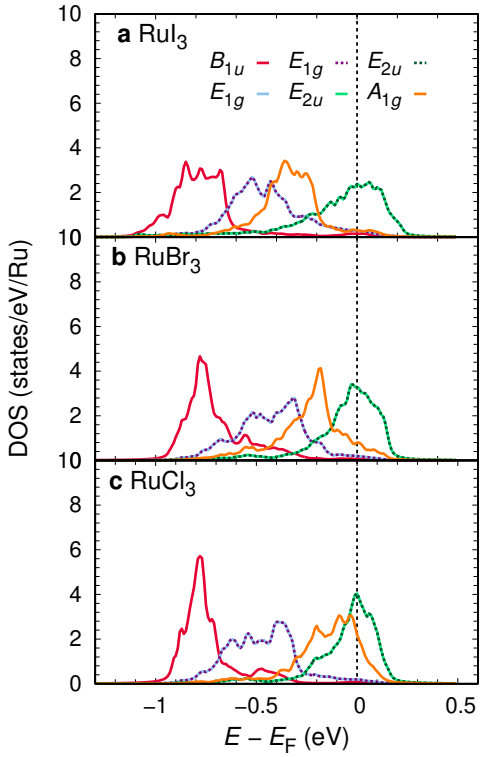

Supplementary Figure 2. **Density of states in the quasimolecular basis.** The DOS was obtained for RuX_3 materials within GGA calculations projected on the quasimolecular (QMO) basis using WIEN2k.

ground state shows no obvious magnetic order, signifying possibly a quantum spin liquid (QSL) state.

Supplementary Note 4: RuX_3 in the quasimolecular orbital basis

In Supplementary Fig. 2 we display the GGA calculations of the DOS for the experimental RuX_3 structures projected on the quasimolecular orbital (QMO) basis [7, 10, 11] that consists of a linear combination of t_{2g} states of the six Ru atoms in a hexagon. Such a calculation provides valuable information on the ligand-Ru hybridizations. We observe that the hopping backbone of the three materials keeps a well defined QMO structure since the GGA results are almost diagonal in this basis. This is a signature that ligand-assisted hopping processes play an important role in all three materials. Interestingly, both $RuBr_3$ (Supplementary Fig. 2b) and RuI_3 (Supplementary Fig. 2c) show almost purely A_{1g} symmetry near the Fermi level in contrast to $RuCl_3$. Such a feature is directly related to the enhanced ligand-assisted hoppings due to the presence of heavier halogens.

Supplementary Note 5: Tabulated values of extracted $j_{eff=1/2}$ models

Tabulated values of the pseudospin models plotted in Fig. 5 of the main text are given in Supplementary Table 3. In addition, we show the model for the $RuCl_3$ $R\bar{3}$ structure, which is very similar to its C2/m counterpart.

Supplementary Note 6: Breakdown of SOC atomic limit

In the Jackeli-Khaliullin mechanism [12] the on-site overlap-integral matrix $\mathbf{\Lambda}$ is usually assumed to follow the form of the so-called SOC atomic limit, such that $\mathbf{\Lambda}\cdot\tilde{\mathbf{S}} = i\,\lambda_{eff}(\mathbf{L}\cdot\tilde{\mathbf{S}})$, where $\mathbf{L}$ is the hydrogen-orbital angular momentum matrix and $\tilde{\mathbf{S}}$ is the electron spin. The $RuCl_3$ $\mathbf{\Lambda}$-matrix roughly follows the atomic limit, shown in Supplementary Table 4 for the z contribution Λ^z. In the same table, we also display the values for the sister compounds with increased halogen atomic number. These RuX_3 values were extracted from Wannier projection of a relativistic band structure calculation (see "Methods" section of the main manuscript). From comparing the four matrices in the table, one can make two important observations: First, with increasing ligand atomic number the matrix element $\Lambda^z_{(xy,x^2-y^2)}$ (usually associated with $2\lambda_{eff}$) rapidly falls, even changing sign between Br and I. Evidently, the SOC effects from magnetic ions and ligands compete in these cases, so that stronger ligand SOC does not directly lead to increased SOC effects in the effective d orbital picture. Second, with higher ligand atomic number, the atomic limit form of the SOC matrix breaks down: In

RuX_3	$RuCl_3$		$RuBr_3$	RuI_3
structure	C2/m	$R\bar{3}$	$R\bar{3}$	$R\bar{3}$
J_1	−2.97	−2.92	−2.91	−0.06
K_1	−5.30	−6.01	−4.04	−5.81
Γ_1	+2.96	+2.69	+2.81	−0.67
Γ'_1	−0.75	−0.87	−0.54	−1.94
J_2	+0.10	+0.10	+0.15	+0.46
K_2	−0.13	−0.14	−0.34	−1.07
Γ_2	+0.05	+0.05	+0.08	+0.57
Γ'_2	+0.05	+0.04	+0.01	+0.19
J_3	+0.11	+0.10	+0.04	−0.08
K_3	+0.07	+0.07	+0.15	+0.31
Γ_3	+0.03	+0.02	+0.04	−0.03
Γ'_3	−0.02	+0.03	−0.06	−0.21
$g_\parallel$	+2.26	+2.26	+2.32	+2.32
$g_\perp$	+1.95	+1.92	+1.88	+1.80

Supplementary Table 3. **Magnetic exchange in the RuX_3 family.** The parameters (in meV) for the experimental structures were extracted using the respective cRPA parameters ($U_{\text{avg}}, J_{\text{avg}}$) for each material. The values for the $C2/m$ structure are C_3-symmetrized (over X, Y, Z bonds). $g_\parallel$ ($g_\perp$) is the contribution to the gyromagnetic tensor $\mathbb{G}$ parallel (perpendicular) to the honeycomb plane.

that limit, the nonzero matrix elements of Λ^z would have a ratio $\Lambda^z_{(xy,x^2-y^2)}/\Lambda^z_{(xz,yz)} = 2$, which is qualitatively satisfied for $RuCl_3$ (ratio ~ 1.4), but not at all for its heavier sister compounds $RuBr_3$ (~ 0.48) and RuI_3 (~ -0.6). Furthermore, additional matrix elements which vanish in the atomic limit become much more relevant for $RuBr_3$ and RuI_3 (see Supplementary Table 4).

[1] Widmann, S. *et al.* Thermodynamic evidence of fractionalized excitations in α-$RuCl_3$. *Phys. Rev. B* **99**, 094415 (2019).

[2] Imai, Y. *et al.* Zigzag magnetic order in the Kitaev spin-liquid candidate material $RuBr_3$ with a honeycomb lattice. *Phys. Rev. B* **105**, L041112 (2022).

[3] Ni, D., Gui, X., Powderly, K. M. & Cava, R. J. Honeycomb-structure RuI_3, a new quantum material related to α-$RuCl_3$. *Adv. Mater.* **34**, 2106831 (2022).

[4] Nawa, K. *et al.* Strongly electron-correlated semimetal RuI_3 with a layered honeycomb structure. *J. Phys. Soc. Japan* **90**, 123703 (2021).

[5] Cao, H. B. *et al.* Low-temperature crystal and magnetic structure of α-$RuCl_3$. *Phys. Rev. B* **93**, 134423 (2016).

[6] Park, S.-Y. *et al.* Emergence of the isotropic Kitaev honeycomb lattice with two-dimensional Ising universality in α-$RuCl_3$. *Preprint at https://arxiv.org/abs/1609.05690* (2016).

[7] Johnson, R. D. *et al.* Monoclinic crystal structure of α-$RuCl_3$ and the zigzag antiferromagnetic ground state. *Phys. Rev. B* **92**, 235119 (2015).

[8] Mu, S. *et al.* Role of the third dimension in searching for Majorana fermions in α-$RuCl_3$ via phonons. *Phys. Rev. Research* **4**, 013067 (2022).

[9] Sears, J. A. *et al.* Ferromagnetic Kitaev interaction and the origin of large magnetic anisotropy in α-$RuCl_3$. *Nat. Phys.* **16**, 837–840 (2020).

[10] Mazin, I. I., Jeschke, H. O., Foyevtsova, K., Valentí, R. & Khomskii, D. I. Na_2IrO_3 as a molecular orbital crystal. *Phys. Rev. Lett.* **109**, 197201 (2012).

[11] Foyevtsova, K., Jeschke, H. O., Mazin, I. I., Khomskii, D. I. & Valentí, R. Ab initio analysis of the tight-binding parameters and magnetic interactions in Na_2IrO_3. *Phys. Rev. B* **88**, 035107 (2013).

[12] Jackeli, G. & Khaliullin, G. Mott Insulators in the Strong Spin-Orbit Coupling Limit: From Heisenberg to a Quantum Compass and Kitaev Models. *Phys. Rev. Lett.* **102**, 017205 (2009).

	atomic limit					**$RuCl_3$**					**$RuBr_3$**					**RuI_3**				
Λ^z	d_{xy}	d_{yz}	d_{z^2}	d_{xz}	$d_{x^2\text{-}y^2}$	d_{xy}	d_{yz}	d_{z^2}	d_{xz}	$d_{x^2\text{-}y^2}$	d_{xy}	d_{yz}	d_{z^2}	d_{xz}	$d_{x^2\text{-}y^2}$	d_{xy}	d_{yz}	d_{z^2}	d_{xz}	$d_{x^2\text{-}y^2}$
d_{xy}	0	0	0	0	$2\,\lambda_{\text{eff}}$	0	−1	0	1	162	0	1	0	5	61	0	−12	1	−5	−75
d_{yz}	0	0	0	λ_{eff}	0	1	0	−0	113	1	−1	0	−4	128	3	12	0	4	126	0
d_{z^2}	0	0	0	0	0	0	0	0	0	1	0	4	0	1	4	−1	−4	0	−10	10
d_{xz}	0	$-\lambda_{\text{eff}}$	0	0	0	−1	−113	0	0	1	−5	−128	−1	0	0	5	−126	10	0	6
$d_{x^2\text{-}y^2}$	$-2\,\lambda_{\text{eff}}$	0	0	0	0	−162	−1	−1	−1	0	−61	−3	−4	−0	0	75	0	−10	−6	0

Supplementary Table 4. **Breakdown of the SOC atomic limit for increasing halogen atomic number.** Comparison of the z-component of the d-orbital on-site overlap matrix $\mathbf{\Lambda}$ in the SOC atomic limit (where $\mathbf{\Lambda}\cdot\tilde{\mathbf{S}} = i\,\lambda_{\text{eff}}\mathbf{L}\cdot\tilde{\mathbf{S}}$) versus *ab-initio* values for RuX_3 (in meV), extracted from relativistic DFT calculations for the indicated compounds.